

# Neutral-Atom Wavelength-Compatible 780 nm Single Photons from a Trapped Ion via Quantum Frequency Conversion

James D. Siverns,<sup>1</sup> John Hannegan,<sup>1</sup> and Qudsia Quraishi<sup>1,2,\*</sup>

<sup>1</sup>*Joint Quantum Institute, University of Maryland, College Park, Maryland 20742, USA*

<sup>2</sup>*Army Research Laboratory, 2800 Powder Mill Road, Adelphi, Maryland 20783, USA*

(Received 22 January 2018; revised manuscript received 16 November 2018; published 23 January 2019)

The interfacing of quantum platforms via photonic links is a precursor for establishing scalable quantum networks. The connection of different types of quantum memories for hybrid networking requires the overcoming of the disparate photon wavelengths emitted by each quantum memory. Given achievements in quantum information processing with trapped-ion and neutral-atom architectures, a hybrid system with modular interconnectivity is advantageous. Here, we use a trapped  $^{138}\text{Ba}^+$  ion and a periodically poled lithium-niobate (PPLN) waveguide, with a fiber-coupled output, to demonstrate 19% end-to-end efficient quantum frequency conversion (QFC) of single photons from 493 to 780 nm and use fluorescence of the ion to produce light at the  $^{87}\text{Rb}$   $D_2$  transition wavelength. To demonstrate the quantum nature of both the unconverted 493 nm photons and the converted photons near 780 nm, we observe strong quantum statistics in their respective second-order intensity correlations. This work extends the range of intralaboratory networking between ions and networking between disparate quantum memories.

DOI: 10.1103/PhysRevApplied.11.014044

## I. INTRODUCTION

Quantum networks consisting of quantum memories and photonic interconnects can be used for entanglement distribution [1,2], quantum teleportation [3], and distributed quantum computing [4]. Remotely connected two-node networks have been demonstrated using memories of the same type: trapped-ion systems [5], quantum dots [6], and nitrogen-vacancy centers [6,7]. Photonic hybrid systems have been demonstrated between a trapped ion and quantum dot [8], single-photon sources and atoms [9–11], and between neutral atoms and both Bose-Einstein condensates [12] and rare-earth-doped crystals [13]. Trapped ions, although a very strong candidate for quantum information [14], have been limited in their use for hybrid photonic systems because the native wavelength is incompatible with most other photon sources.

Trapped ions [15,16] and neutral atoms [17,18] are both well-advanced quantum systems and have the important advantage of comparable photon temporal features that are useful for interfacing them together [19]. The integration of these two platforms via a hybrid network allows the strengths of each system to be used individually while, simultaneously, allowing for new avenues to be explored, such as hybrid quantum networking via entanglement distribution and photon storage, as well

as photonic quantum computation using converted ion-photons and neutral atoms coupled to optical cavities [20,21]. However, to perform such hybrid quantum networking experiments using photonic interconnects, the photons emitted from both systems need to have the same optical frequency. In this work, we solve this critical problem, which prevents two systems with disparate wavelengths from interacting, by demonstrating the conversion of 493 nm photons, emitted from a single barium ion, to a 780 nm wavelength equal to the  $D_2$  transition in neutral  $^{87}\text{Rb}$ .

A secondary benefit of the conversion process is the ability to significantly extend the networking range between trapped-ion nodes. Trapped ions perform extremely well as quantum nodes in terms of photon generation and detection [5,22], quantum computation [14,23–25], and single-photon emission [26]. However they are limited in the distance between nodes due to their native emission frequencies. In the case of  $\text{Ba}^+$ , the fiber attenuation is 50 dB/km at 493 nm, whereas its frequency-converted photon, in the near-infrared range, would experience an attenuation of 3.5 dB/km, thereby allowing the distance between two ion-based quantum nodes to be increased for the same level of total attenuation. This work, therefore, provides a twofold benefit of paving the way for neutral-ion hybrid networking and communication as well as extending the networking capability of barium ions from 100s of meters to several kilometers, allowing for both an ion-ion and neutral-ion quantum intranet [27].

\*quraishi@umd.edu

## II. METHODS AND EXPERIMENTAL DETAILS

Quantum frequency conversion (QFC) [28], in a periodically poled lithium-niobate (PPLN) waveguide, frequency converts a photon of one frequency to another while preserving its quantum properties [29–31]. PPLNs provide a modular component for integration in a quantum network [32]. Using a three-wave parametric  $\chi^{(2)}$  nonlinearity, QFC generates an output photon via optical difference-frequency generation (DFG) between a pump and an input photon. By selecting a pump frequency lower than the desired output frequency, we can minimize noise photons at undesired optical frequencies resulting from spontaneous parametric downconversion and anti-Stokes Raman processes [33].

As shown in Fig. 1(a), a single  $^{138}\text{Ba}^+$  ion is trapped using electrodes in a blade-trap configuration, which is housed in an ultra-high-vacuum chamber on the ion table [27]. Windows in the vacuum chamber allow for two collection lenses, each with a numerical aperture (NA) of 0.4, to collect ion fluorescence from both sides of the chamber simultaneously. The windows are antireflection coated and the total fluorescence collection is approximately 8% at 493 nm. Collection lens A directs free-space light into a photomultiplier tube (PMT), with a specified quantum efficiency (QE) of around 6% (Hamamatsu H11870-01) at 493 nm, via a doublet lens, a 493 nm notch filter, and an iris. The  $^{138}\text{Ba}^+$  ion is Doppler cooled with 493 nm light on the  $^2S_{1/2}$ - $^2P_{1/2}$  transition and repumped out of the metastable  $^2D_{3/2}$  state with light near 650 nm.

The Doppler- and repump-beam frequencies are stabilized to an optical wavelength meter to approximately

2 MHz. With this setup, we observe a maximized fluorescence rate from the ion of approximately 20 800 counts/s using the PMT. Photons collected via lens B are sent into a single-mode fiber (SMF) with a coupling efficiency of approximately 17% and then sent either directly to an avalanche photon detector (APD) (Perkin Elmer SPCM-AQR-15) with a QE of approximately 45% at 493 nm or to the frequency-conversion setup [Fig. 1(b)], where they are converted to 780 nm and sent to the APD, with a specified QE of approximately 60% at 780 nm. When sent directly to the APD, the measured 493 nm photon count rate is approximately 26 600 counts/s.

The frequency-conversion setup shown in Fig. 1(b) spatially combines the 493 nm light and the 1343 nm pump using a dichroic mirror. A  $\times 20$  objective lens then focuses the combined beams onto the PPLN waveguide (Srico 2000-1004). The PPLN output facet couples directly into a polarization-maintaining SMF designed for use near 800 nm. Light out of the PPLN fiber is free-space coupled to allow for 70 dB of pump filtering and 59 dB of nonconverted 493 nm leak-through filtering using a filter set (ThorLabs FBH780-10 and two Semrock FF01-1326/SP-25).

## III. RESULTS

### A. The quantum-frequency-conversion efficiency and tunability

To determine the QFC efficiency of the PPLN setup, a 493 nm laser, locked to 607.425690(2) THz, and a pump at 1343 nm are used as inputs to the PPLN waveguide.

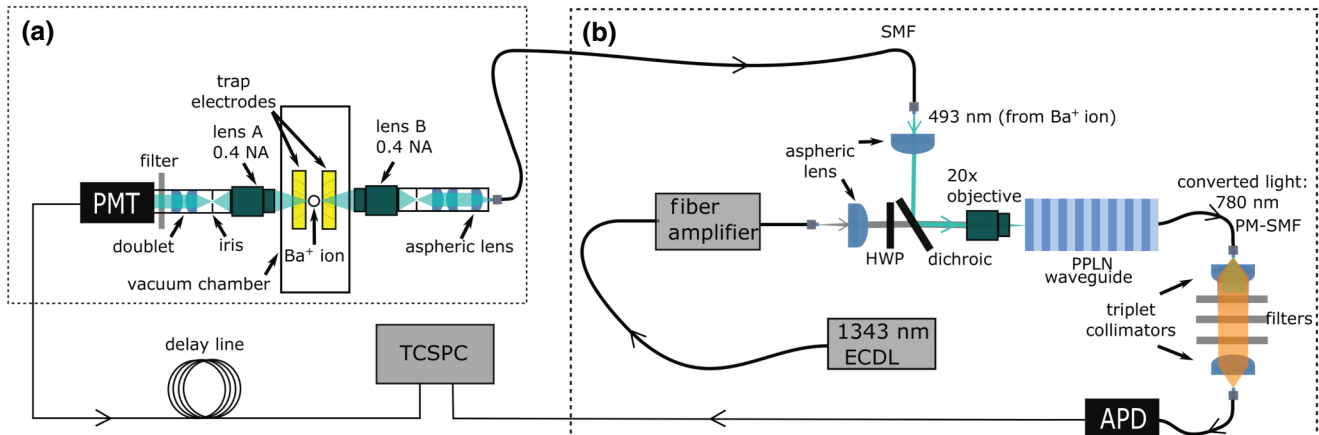


FIG. 1. (a) A schematic of the trapped-ion setup, showing two separate optical collection paths that are situated on opposite sides of an ultra-high-vacuum chamber. The vacuum windows are antireflection coated and allow optical access for two 0.4 numerical aperture (NA) objectives, lens A and lens B. The 493 nm photons collected by lens B are collimated and launched into a single-mode fiber (SMF) of a few meters in length. A photomultiplier tube (PMT) measures the photons collected by lens A. (b) The quantum-frequency-conversion (QFC) setup, including a half-wave plate (HWP) and a dichroic mirror that combines 493 nm and pump photons. A  $\times 20$  objective couples the combined light into a periodically poled lithium-niobate (PPLN) waveguide with a small length of polarization-maintaining single-mode fiber (PM-SMF) butt-coupled to its output facet. The light emitted from this fiber is free-space propagated to allow for the use of optical filters and then recoupled into a standard SMF, a few meters in length, for detection by an avalanche photodiode (APD). Photon-detection events are monitored using a time-correlated two-channel single-photon counter (TCSPC).

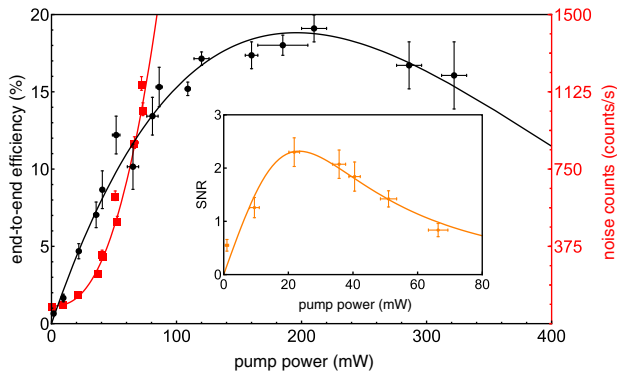


FIG. 2. The end-to-end conversion efficiency of the DFG from 493 to 780 nm (black circles and left-hand axis) and noise produced in the bandwidth allowed by our filtering (red squares and right-hand axis) as a function of the pump power coupled into the waveguide. The inset shows the signal-to-noise ratio (SNR) of the conversion process for the case where the signal is from the fiber-coupled ion light, as described in the main text. The error bars on the pump power are from fluctuations of the measured power and the error bars on the efficiency are primarily from DFG signal-power fluctuations.

The pump power is varied while the DFG optical power is measured after the filters. The end-to-end efficiency is determined by taking the ratio of the measured DFG power to the 493 nm power sent to the device, while correcting for the change in frequency. The end-to-end conversion efficiency depends on the pump power coupled into the waveguide, as shown in Fig. 2, with a maximum of approximately 19% at a coupled pump power of approximately 210 mW. The efficiency is largely limited by the coupling (approximately 30%) of the 493 nm light into the PPLN.

To facilitate hybrid interactions, it is important that the PPLN DFG output be tunable to resonance with the  $^{87}\text{Rb}$   $D_2$  transition at 384.228 THz [34], while at the same time the input frequency needs to be resonant with the barium ion. This double-resonance condition gives two constraints that are met by identifying appropriate pump-wavelength and PPLN-oven-temperature operation points. To determine these values, the DFG output is maximized at a pump wavelength near 1336 nm at a PPLN oven temperature of  $35.5^\circ\text{C}$ . The wavelength of the DFG is then tuned to that of the  $^{87}\text{Rb}$   $D_2$  line by increasing the pump wavelength to a value of 1343.169 nm and tuning the PPLN temperature to  $43^\circ\text{C}$ . All of the tuning is carried out with the 493 nm laser locked to  $\text{Ba}^+$  resonance. Fine tuning of the DFG signal frequency is possible by adjusting the pump wavelength, as shown in Fig. 3.

While operating at the maximum conversion efficiency increases the number of 780 nm photons produced, the larger pump power required results in increased production of anti-Stokes noise photons. Therefore, when frequency converting light from the ion, it is critical to chose a pump power that is close to the maximum signal-to-noise ratio

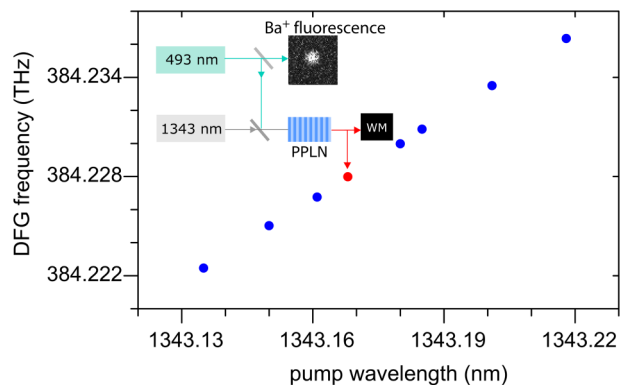


FIG. 3. The DFG output frequency as a function of the pump wavelength near 1343 nm. The inset is a block diagram of the setup, showing simultaneous resonant-ion fluorescence when the  $\text{Ba}^+$  ion Doppler-cooling laser ( $^2\text{S}_{1/2}$ - $^2\text{P}_{1/2}$  transition) is locked to 607.425690(2) THz while the DFG PPLN output is at the  $^{87}\text{Rb}$   $D_2$  line frequency of 384.227982(2) THz [34] (red data point), as measured to a 2 MHz accuracy using a wavelength meter (WM) (HighFinesse WSU/2). The PPLN temperature is held at a constant temperature of  $43^\circ\text{C}$  during this procedure.

(SNR) of the DFG light. Figure 2 shows the noise inside the bandwidth of the filters as a function of the pump power coupled into the waveguide as well as the resulting SNR (see the inset of Fig. 2) for the case of a signal from fiber-coupled ion fluorescence.

For single-photon measurements, we use a value of the pump power that corresponds to a near optimal SNR (shown in the inset of Fig. 2) and the pump wavelength and oven temperature shown in Fig. 3. With approximately 40 mW of pump light coupled into the waveguide, we measure a total noise level of approximately 300 counts/s on the APD, which includes an APD detector dark-count rate of approximately 100 counts/s. We measure no pump leakage through the filters, as when the PPLN is bypassed only APD dark counts are observed. Therefore, counts above the APD dark-count rate are attributable to anti-Stokes Raman photons produced by the pump within the filtering wavelength range of  $780 \pm 5$  nm. Importantly, there are no detectable levels of 493 or 650 nm ion light making it through the filters by observing count rates equal to that of the APD dark counts when only the ion light is present. Therefore, any subunitary second-order intensity-correlation measurements detected between events on the APD and the PMT can only be caused by correlations between frequency-converted 780 nm photons (at the APD) and unconverted 493 nm photons (at the PMT).

When both 493 nm photons from the ion and the 40 mW pump light are present in the PPLN waveguide, the measured count rate of the 780 nm DFG light is approximately 600 counts/s, giving a SNR of approximately 2. A conversion efficiency of approximately 2.3%, including all optical and fiber-coupling losses, is determined by taking the ratio

of the converted photon count rate to the 493 nm photon count rate as measured directly on the APD (approximately 26 100 counts/s). Taking into account a factor-of-2 loss in a fiber patch cable between the ion and QFC tables, another factor-of-2 loss for polarization selectivity of the QFC process, and other optical losses, this value is consistent with the classically measured value shown in Fig. 2.

### B. Single-photon statistics

The measurement of the  $g^{(2)}(\tau)$  correlation function of single photons produced by the  $\text{Ba}^+$  ion is performed using the light collected from two sides of the ion, as a function of the relative delay,  $\tau$ , between detection events on either side. This approach is equivalent to a Hanbury Brown–Twiss apparatus, in which the ion can be treated as the beam splitter. The photons are collected while continuously Doppler cooling the ion. The measurement is performed first between non-frequency-converted 493 nm photons emitted by the ion and then between non-frequency-converted photons and frequency-converted 780 nm photons. A PMT is used to detect the 493 nm photons collected by lens A and these detection events are correlated with the APD-detected photons collected by lens B, either directly from the ion or via the frequency-conversion setup [shown in Fig. 1(b)].

The output of each detector is sent to a time-correlated two-channel single-photon counter (TCSPC) with a resolution of 512 ps (PicoQuant PicoHarp 300). Using the counter's histogram mode, the arrival of a pulse from the PMT triggers a timing circuit that measures the time until a pulse is received from the APD. An electrical delay line is added to the PMT line to allow the measurement of negative delay times. The time between pulses on each detector is then binned into 512-ps-wide bins. To calculate the  $g^{(2)}(\tau)$ , the raw coincidence counts are normalized using [35,36]

$$g^{(2)}(\tau) = \frac{N(\tau)}{N_{\text{PMT}} N_{\text{APD}} \delta_t T}. \quad (1)$$

Here,  $N(\tau)$  is the number of coincidence counts in a bin,  $\delta_t$  is the size of the time bin (512 ps),  $T$  is the total integration time, and  $N_{\text{PMT}}$  and  $N_{\text{APD}}$  are the total count rates in the PMT and APD channels, respectively. The normalized and delay-line-compensated  $g^{(2)}(\tau)$  measured between non-converted photons (blue) and converted and nonconverted photons (red) are shown in Fig. 4. The insets show the raw coincidence-count data with the electronic delays of 91.65 and 53.76 ns present. The periodic oscillation of the counts is due to micromotion of the ion in the trap at a frequency of  $\Omega/2\pi = 38.4$  MHz. The measured  $g^{(2)}(0)$  of 493 nm photons directly emitted by the ion and between 493 nm photons and frequency-converted 780 nm photons are measured to be  $0.167 \pm 0.022$  and  $0.645 \pm 0.055$ , respectively.

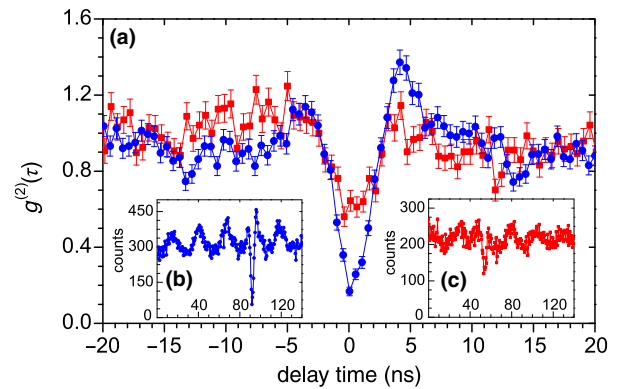


FIG. 4. (a) The  $g^{(2)}(\tau)$  correlation function measured between non-frequency-converted 493 nm photons (blue), where  $g^{(2)}(0) = 0.167 \pm 0.022$ , and between 493 nm and converted 780 nm photons (red), where  $g^{(2)}(0) = 0.645 \pm 0.055$ . These measurements agree with the expected values given by Eq. (2), given that  $\delta_t = 512$  ps. The error bars represent the shot noise from each detector. The insets show the raw unnormalized coincidence counts, where (b)  $N_{\text{APD}} = 26\,600$  counts/s,  $N_{\text{PMT}} = 19\,700$  counts/s, and  $T = 20$  min and (c)  $N_{\text{APD}} = 930$  counts/s,  $N_{\text{PMT}} = 20\,500$  counts/s, and  $T = 6.13$  h.

In a noiseless  $g^{(2)}(\tau)$  measurement with infinitely small bin widths, zero coincident counts are expected at  $\tau = 0$  from a single-photon source such as an ion. Experimentally, however, a finite bin width must be used and noise-detector clicks are inevitable. The finite bin width is used to calculate a minimum  $g^{(2)}(0)$  of  $a = 0.035$ , using the methods described in [35]. To take the effects of noise and the finite bin width into account, the following is used [37]:

$$g_{\text{exp}}^{(2)}(t) = 1 + \left( \frac{\text{SNR}}{1 + \text{SNR}} \right)^2 (a - 1), \quad (2)$$

where SNR is the ratio of the histogram counts per second due to the signal from the ion to the histogram counts per second due to correlations with noise. The latter include PMT-noise–APD-noise correlations, PMT-signal–APD-noise correlations, and PMT-noise–APD-signal correlations.

For the correlation measurement solely between the unconverted 493 nm photons from the ion, the main noise sources are from correlations between the PMT signal and the APD noise and between the PMT noise and the APD signal. The histogram count rates from each of these sources are measured to be 276 counts/s and 359 counts/s, respectively. With the inclusion of a small PMT-noise–APD-noise contribution (6 counts/s), a total noise rate of 641 counts/s is measured. Given a total histogram count rate of 10 800 counts/s, a SNR of 15.8 is achieved. The expected  $g_{\text{exp}}^{(2)}(0)$  is therefore found to be 0.146. This

value is in agreement with the measured value of  $0.167 \pm 0.022$ .

The measurement between the unconverted 493 nm photons and converted 780 nm photons has noise counts that are dominated by correlations between signal PMT counts and APD noise counts. The measured histogram count rate due to such correlations is found to be 200 counts/s and the other noise sources produce a combined 20 counts/s. With a total count rate of 615 counts/s, this corresponds to a SNR of 1.80. The measured value of  $g^{(2)}(0)$  is found to be  $0.645 \pm 0.055$ , in agreement with the expected value of 0.602, and also significantly below the classical limit, demonstrating the conversion of single photons from 493 to 780 nm.

During the course of this work, other groups have converted photons from a  $\text{Ca}^+$  to 1530 nm, preserving their quantum statistics [38] and, separately, to 1310 nm, with the demonstration of ion-photon entanglement [39].

#### IV. CONCLUSION

We demonstrate the conversion of photons from a single trapped ion into optical frequencies that are compatible with a neutral atomic system. For quantum networking, it is important to be able to extract flying qubits [40] and have a long-lived qubit—such as a potentially long-lived hyperfine qubit in  $^{133}\text{Ba}^+$  [41]. The conversion of photons emitted from a trapped ion into the near-infrared provides the ability to network ions over significantly larger distances than is achievable with their native wavelengths due to decreased losses in optical fibers. This result paves the way for ion-ion and hybrid-species quantum networking.

#### ACKNOWLEDGMENTS

This work is supported by the Center for Distributed Quantum Information (CDQI) and the Army Research Laboratory Open Campus Initiative.

- [1] L.-M. Duan and H. J. Kimble, Efficient Engineering of Multiatom Entanglement Through Single-Photon Detections, *Phys. Rev. Lett.* **90**, 253601 (2003).
- [2] H. J. Kimble, The quantum internet, *Nature* **453**, 1023 (2008).
- [3] S. Pirandola, J. Eisert, C. Weedbrook, A. Furusawa, and S. L. Braunstein, Advances in quantum teleportation, *Nat. Photon.* **9**, 641 (2015).
- [4] T. P. Spiller, Kae Nemoto, Samuel L. Braunstein, W. J. Munro, P. van Loock, and G. J. Milburn, Quantum computation by communication, *New J. Phys.* **8**, 30 (2006).
- [5] D. Hucul, I. V. Inlek, G. Vittorini, C. Crocker, S. Debnath, S. M. Clark, and C. Monroe, Modular entanglement of atomic qubits using photons and phonons, *Nat. Phys.* **11**, 37 (2014).
- [6] W. B. Gao, A. Imamoglu, H. Bernien, and R. Hanson, Coherent manipulation, measurement and entanglement of individual solid-state spins using optical fields, *Nat. Photon.* **9**, 363 (2015).
- [7] B. Hensen, H. Bernien, A. E. Dréau, A. Reiserer, N. Kalb, M. S. Blok, J. Ruitenberg, R. F. L. Vermeulen, R. N. Schouten, C. Abellán, W. Amaya, V. Pruneri, M. W. Mitchell, M. Markham, D. J. Twitchen, D. Elkouss, S. Wehner, T. H. Taminiau, and R. Hanson, Loophole-free Bell inequality violation using electron spins separated by 1.3 kilometres, *Nature* **526**, 682 (2015).
- [8] H. M. Meyer, R. Stockill, M. Steiner, C. Le Gall, C. Matthiesen, E. Clarke, A. Ludwig, J. Reichel, M. Atatüre, and M. Köhl, Direct Photonic Coupling of a Semiconductor Quantum Dot and a Trapped Ion, *Phys. Rev. Lett.* **114**, 123001 (2015).
- [9] N. Akopian, L. Wang, A. Rastelli, O. G. Schmidt, and V. Zwiller, Hybrid semiconductor-atomic interface: Slowing down single photons from a quantum dot, *Nat. Photon.* **5**, 230 (2011).
- [10] Petr Siyushev, Guilherme Stein, Jörg Wrachtrup, and Ilja Gerhardt, Molecular photons interfaced with alkali atoms, *Nature* **509**, 66 (2014).
- [11] Han Zhang, Xian-Min Jin, Jian Yang, Han-Ning Dai, Sheng-Jun Yang, Tian-Ming Zhao, Jun Rui, Yu He, Xiao Jiang, and Fan Yang *et al.*, Preparation and storage of frequency-uncorrelated entangled photons from cavity-enhanced spontaneous parametric downconversion, *Nat. Photon.* **5**, 628 (2011).
- [12] M. Lettner, M. Mücke, S. Riedl, C. Vo, C. Hahn, S. Baur, J. Bochmann, S. Ritter, S. Dürr, and G. Rempe, Remote Entanglement Between a Single Atom and a Bose-Einstein Condensate, *Phys. Rev. Lett.* **106**, 210503 (2011).
- [13] Nicolas Maring, Pau Farrera, Kutlu Kutluer, Margherita Mazzera, Georg Heinze, and Hugues de Riedmatten, Photonic quantum state transfer between a cold atomic gas and a crystal, *Nature* **551**, 485 (2017).
- [14] Norbert M. Linke, Dmitri Maslov, Martin Roetteler, Shantanu Debnath, Caroline Figgatt, Kevin A. Landsman, Kenneth Wright, and Christopher Monroe, Experimental comparison of two quantum computing architectures, *Proc. of the Nat. Acad. of Sci.* **114**, 3305 (2017).
- [15] James D. Sivers and Qudsia Quraishi, Ion trap architectures and new directions, *Quantum Inf. Process.* **16**, 314 (2017).
- [16] C. Monroe, R. Raussendorf, A. Ruthven, K. R. Brown, P. Maunz, L.-M. Duan, and J. Kim, Large-scale modular quantum-computer architecture with atomic memory and photonic interconnects, *Phys. Rev. A* **89**, 022317 (2014).
- [17] H.-J. Briegel, T. Calarco, D. Jaksch, J. I. Cirac, and P. Zoller, Quantum computing with neutral atoms, *J. Modern Opt.* **47**, 415 (2000).
- [18] Ivan H. Deutsch, Gavin K. Brennen, and Poul S. Jessen, Quantum computing with neutral atoms in an optical lattice, *Fortschritte Phys.* **48**, 925 (2000).
- [19] A. M. Dyckovsky and S. Olmschenk, Analysis of photon-mediated entanglement between distinguishable matter qubits, *Phys. Rev. A* **85**, 052322 (2012).
- [20] Andreas Reiserer, Norbert Kalb, Gerhard Rempe, and Stephan Ritter, A quantum gate between a flying optical photon and a single trapped atom, *Nature* **508**, 237 (2014).

- [21] L.-M. Duan and H. J. Kimble, Scalable Photonic Quantum Computation Through Cavity-Assisted Interactions, *Phys. Rev. Lett.* **92**, 127902 (2004).
- [22] Kenneth R. Brown, Jungsang Kim, and Christopher Monroe, Co-designing a scalable quantum computer with trapped atomic ions, *NPJ Q. Info.* **2**, 16034 (2016).
- [23] A. Bermudez, X. Xu, R. Nigmatullin, J. O’Gorman, V. Negnevitsky, P. Schindler, T. Monz, U. G. Poschinger, C. Hempel, J. Home, F. Schmidt-Kaler, M. Biercuk, R. Blatt, S. Benjamin, and M. Müller, Assessing the Progress of Trapped-Ion Processors Towards Fault-Tolerant Quantum Computation, *Phys. Rev. X* **7**, 041061 (2017).
- [24] C. J. Ballance, V. M. Schäfer, J. P. Home, D. J. Szwer, S. C. Webster, D. T. C. Allcock, N. M. Linke, T. P. Harty, D. P. L. Aude Craik, D. N. Stacey, A. M. Steane, and D. M. Lucas, Hybrid quantum logic and a test of Bell’s inequality using two different atomic isotopes, *Nature* **528**, 384 (2015).
- [25] T. R. Tan, J. P. Gaebler, Y. Lin, Y. Wan, R. Bowler, D. Leibfried, and D. J. Wineland, Multi-element logic gates for trapped-ion qubits, *Nature* **528**, 380 (2015).
- [26] D. B. Higginbottom, L. Slodička, G. Araneda, L. Lachman, R. Filip, M. Hennrich, and R. Blatt, Pure single photons from a trapped atom source, *New J. Phys.* **18**, 093038 (2016).
- [27] J. D. Siverns, X. Li, and Q. Quraishi, Ion-photon entanglement and quantum frequency conversion with trapped Ba<sup>+</sup> ions, *Appl. Opt.* **56**, B222 (2017).
- [28] Prem Kumar, Quantum frequency conversion, *Opt. Lett.* **15**, 1476 (1990).
- [29] Andreas Lenhard, José Brito, Matthias Bock, Christoph Becher, and Jürgen Eschner, Coherence and entanglement preservation of frequency-converted heralded single photons, *Opt. Exp.* **25**, 11187 (2017).
- [30] Serkan Ates, Imad Agha, Angelo Gulinatti, Ivan Rech, Matthew T. Rakher, Antonio Badolato, and Kartik Srinivasan, Two-Photon Interference Using Background-Free Quantum Frequency Conversion of Single Photons Emitted by an InAs Quantum Dot, *Phys. Rev. Lett.* **109**, 147405 (2012).
- [31] Rikizo Ikuta, Yoshiaki Kusaka, Tsuyoshi Kitano, Hiroshi Kato, Takashi Yamamoto, Masato Koashi, and Nobuyuki Imoto, Wide-band quantum interface for visible-to-telecommunication wavelength conversion, *Nat. Commun.* **2**, 1544 (2011).
- [32] Nicolas Maring, Pau Farrera, Kutlu Kutluer, Margherita Mazzera, Georg Heinze, and Hugues de Riedmatten, Photonic quantum state transfer between a cold atomic gas and a crystal, *Nature* **551**, 485 (2017).
- [33] J. S. Pelc, L. Ma, C. R. Phillips, Q. Zhang, C. Langrock, O. Slattery, X. Tang, and M. M. Fejer, Long-wavelength-pumped upconversion single-photon detector at 1550 nm: Performance and noise analysis, *Opt. Exp.* **19**, 21445 (2011).
- [34] Jun Ye, Steve Swartz, Peter Jungner, and John L. Hall, Hyperfine structure and absolute frequency of the <sup>87</sup>Rb 5P<sub>3/2</sub> state, *Opt. Lett.* **21**, 1280 (1996).
- [35] G. Muñoz-Matutano, D. Barrera, C. R. Fernández-Pousa, R. Chulia-Jordan, L. Seravalli, G. Trevisi, P. Frigeri, S. Sales, and J. Martínez-Pastor, All-optical fiber Hanbury Brown & Twiss interferometer to study 1300 nm single photon emission of a metamorphic InAs quantum dot, *Sci. Rep.* **6**, 27214 (2016).
- [36] Rosa Brouri, Alexios Beveratos, Jean-Philippe Poizat, and Philippe Grangier, Photon antibunching in the fluorescence of individual color centers in diamond, *Opt. Lett.* **25**, 1294 (2000).
- [37] C. Becher, A. Kiraz, P. Michler, A. Imamoglu, W. V. Schoenfeld, P. M. Petroff, Lidong Zhang, and E. Hu, Nonclassical radiation from a single self-assembled InAs quantum dot, *Phys. Rev. B* **63**, 121312 (2001).
- [38] Thomas Walker, Koichiro Miyanishi, Rikizo Ikuta, Hiroki Takahashi, Samir Vartabi Kashanian, Yoshiaki Tsujimoto, Kazuhiro Hayasaka, Takashi Yamamoto, Nobuyuki Imoto, and Matthias Keller, Long-Distance Single Photon Transmission from a Trapped Ion via Quantum Frequency Conversion, *Phys. Rev. Lett.* **120**, 203601 (2018).
- [39] Matthias Bock, Pascal Eich, Stephan Kucera, Matthias Kreis, Andreas Lenhard, Christoph Becher, and Jürgen Eschner, High-fidelity entanglement between a trapped ion and a telecom photon via quantum frequency conversion, *Nat. Commun.* **9**, 1998 (2018).
- [40] Chen-Kuan Choua, Carolyn Auchter, Jennifer Lilieholm, Kevin Smith, and Boris Blinov, Single ion imaging and fluorescence collection with a parabolic mirror trap, *Rev. Sci. Inst.* **88**, 086101 (2017).
- [41] David Hucul, Justin E. Christensen, Eric R. Hudson, and Wesley C. Campbell, Spectroscopy of a Synthetic Trapped Ion Qubit, *Phys. Rev. Lett.* **119**, 100501 (2017).